



A Novel SXT/R391 Integrative and Conjugative Element Carries Two Copies of the *bla*_{NDM-1} Gene in *Proteus mirabilis*

Jintao He,^{a,b,c} Long Sun,^d Linghong Zhang,^{a,b,c} Sebastian Leptihn,^{a,e} Yunsong Yu,^{a,b,c}  Xiaoting Hua^{a,b,c}

^aDepartment of Infectious Diseases, Sir Run Run Shaw Hospital, Zhejiang University School of Medicine, Hangzhou, China

^bKey Laboratory of Microbial Technology and Bioinformatics of Zhejiang Province, Hangzhou, China

^cRegional Medical Center for National Institute of Respiratory Diseases, Sir Run Run Shaw Hospital, School of Medicine, Zhejiang University, Hangzhou, China

^dDepartment of Clinical Laboratory, Hangzhou Women's Hospital, Hangzhou Maternity and Child Health Care Hospital, Hangzhou, China

^eZhejiang University, Haining, China

Jintao He and Long Sun contributed equally to this work. Author order was determined by type of contribution.

ABSTRACT The rapid spread of the *bla*_{NDM-1} gene is a major public health concern. Here, we describe the multidrug-resistant *Proteus mirabilis* strain XH1653, which contains a novel SXT/R391 integrative and conjugative element (ICE), harboring two tandem copies of *bla*_{NDM-1} and 21 other resistance genes. XH1653 was resistant to all antibiotics tested, apart from aztreonam. Whole-genome data revealed that two copies of *bla*_{NDM-1} embedded in the *ISCR1* element are located in HS4 of the novel ICE, which we named ICEPmiChnXH1653. A circular intermediate of ICEPmiChnXH1653 was detected by PCR, and conjugation experiments showed that the ICE can be transferred to the *Escherichia coli* strain EC600 with frequencies of 1.5×10^{-7} . In the recipient strain, the ICE exhibited a higher excision frequency and extrachromosomal copy number than the ICE in the donor strain. We also observed that the presence of ICEPmiChnXH1653 has a negative impact on bacterial fitness and leads to changes in the transcriptome of the host. *In vitro* evolution experiments under nonselective conditions showed that the two tandem copies of the *ISCR1* element and the *ISVsα3* element can be lost during repeated laboratory passage. This is the first report of a novel SXT/R391 ICE carrying two tandem copies of *bla*_{NDM-1}, which also illustrates the role that ICEs may play as platforms for the accumulation and transmission of antibiotic resistance genes.

IMPORTANCE The occurrence of carbapenemase-producing *Proteus mirabilis*, especially those strains producing NDM-1 and its variants, is a major public health concern worldwide. The integrative conjugative element (ICE) plays an important role in horizontal acquisition of resistance genes. In this study, we characterized a novel SXT/R391 ICE from a clinical *P. mirabilis* isolate that we named ICEPmiChnXH1653, which contains two tandem copies of the carbapenemase gene *bla*_{NDM-1}. We performed an integrative approach to gain insights into different aspects of ICEPmiChnXH1653 evolution and biology and observed that ICEPmiChnXH1653 obtained the carbapenemase gene *bla*_{NDM-1} by *ISCR1*-mediated homologous recombination. Our study reveals that the transmission of *bla*_{NDM-1} by *ISCR1* elements or ICEs may be an important contributor to the carbapenem resistance development across species, which could improve our understanding of horizontal gene transfer in clinical environments.

KEYWORDS *Proteus mirabilis*, SXT/R391, ICE, tandem copies, *bla*_{NDM-1}, *ISCR1*

The Gram-negative bacillus *Proteus mirabilis* is emerging as an increasingly important pathogen in nosocomial infections, particularly in urinary tract infections (1). Due to intrinsic resistance to nitrofurantoin, polymyxin, and tigecycline, the occurrence

Citation He J, Sun L, Zhang L, Leptihn S, Yu Y, Hua X. 2021. A novel SXT/R391 integrative and conjugative element carries two copies of the *bla*_{NDM-1} gene in *Proteus mirabilis*. *mSphere* 6: e00588-21. <https://doi.org/10.1128/mSphere.00588-21>.

Editor Patricia A. Bradford, Antimicrobial Development Specialists, LLC

Copyright © 2021 He et al. This is an open-access article distributed under the terms of the [Creative Commons Attribution 4.0 International license](https://creativecommons.org/licenses/by/4.0/).

Address correspondence to Yunsong Yu, yvys119@zju.edu.cn, or Xiaoting Hua, xiaotinghua@zju.edu.cn.

Received 29 June 2021

Accepted 29 July 2021

Published 11 August 2021

of carbapenemase-producing *P. mirabilis* is of particular concern; in particular, strains producing the New Delhi metallo- β -lactamase 1 (NDM-1) make treatment extremely difficult (2, 3). NDM-1, an Ambler class B β -lactamase, is the main type of carbapenemase, conferring resistance to almost all β -lactams except monobactams (4). Global dissemination of NDM-1 is a major public health problem (5, 6). bla_{NDM-1} is a chimeric gene that has arisen by a gene fusion event linking the aminoglycoside resistance gene *aphA6* to a preexisting metallo- β -lactamase (MBL) gene and is frequently located downstream of a complete or truncated copy of *ISAbal25* (7). The bla_{NDM-1} gene has been found in various genetic contexts including prophages (8) but is most often associated with other mobile genetic elements that are responsible for its evolution and rapid transmission (9). For instance, ISCRs (insertion sequences with a common region) are often found in the vicinity of bla_{NDM-1} and considered one of the routes of the fusion of bla_{NDM-1} and also involved in the mobilization of bla_{NDM-1} (7, 9–11). In addition, horizontal dissemination of bla_{NDM-1} among diverse species can occur via mobile DNA vectors, mostly conjugative plasmids and integrative conjugative elements (ICEs) (12, 13).

ICEs are self-transmissible mobile genetic elements which encode modules that facilitate integration/excision, conjugative transfer, and maintenance (14). The element can therefore be excised from the host chromosome to form a circular intermediate that can be transferred to a recipient cell via conjugation (15). The SXT/R391 family, one of the largest families of ICEs, has a highly conserved core of sequences that mediate the site-specific integration into the 5' end of the *prfC* gene (14, 16). Except for a conserved backbone, SXT/R391 ICEs frequently contain hot spots (HS1 to HS5) and variable regions (VRI to VRV) that carry genes for antimicrobial resistance and metal tolerance (17, 18). Many SXT/R391 ICEs have been found in *P. mirabilis*, contributing to the dissemination of antimicrobial resistance genes (ARGs) including the cephalosporinase gene bla_{CMY-2} (19–21). Most recently, an SXT/R391 ICE carrying the carbapenemase gene bla_{NDM-1} embedded within a truncated *Tn125* was identified in *Proteus vulgaris* (13).

In this study, we characterized a novel SXT/R391 ICE from a *P. mirabilis* isolate, named ICEPmiChnXH1653, which contains two tandem copies of bla_{NDM-1} and 21 other ARGs. An integrative approach, combining bacterial conjugation tests, fitness assays, experimental evolution, genomics, and transcriptomics, allowed us to gain insights into diverse aspects of evolution and biology of ICEPmiChnXH1653 (22).

RESULTS

Characterization of bla_{NDM-1} -bearing *P. mirabilis* strain XH1653. While being intrinsically resistant to tetracycline and colistin, the *P. mirabilis* strain XH1653 exhibited resistance to all tested antimicrobials with the exception of aztreonam, thus defining the strain as multi-/extensively drug resistant (MDR/XDR). The strain contains a single circular chromosome with a size of 4,113,626 bp (GC content 39.2%). We identified multiple ARGs including those for β -lactams (bla_{NDM-1} , $bla_{CTX-M-65}$, bla_{OXA-1}), fluoroquinolone [*aac(6')-Ib-cr*], fosfomicin (*fosA3*), tetracycline [*tet(C)*, *tet(J)*], aminoglycosides [*aadA2*, *aph(4)-Ia*, *strB*, *strA*, *aac(6')-Ib-cr*, *aphA*, *aac(3)-IVa*], sulfamethoxazole (*sul1*, *sul2*), trimethoprim (*dfrA32*), phenicol (*catB3*, *floR*, *catA4*), rifamycin (*arr-3*), macrolide [*ere(A)*, *erm(42)*], and bleomycin (ble_{MBL} , *bleO*). Interestingly, we found that XH1653 contains two copies of the carbapenemase gene bla_{NDM-1} . To corroborate this finding, we employed real-time quantitative PCR (qPCR) to determine the number of copies of bla_{NDM-1} per cell, which confirmed the presence of multiple copies of bla_{NDM-1} (2.79 ± 0.67 copies/cell) (Fig. 1A). Further sequence analysis showed that all ARGs, with the exception of *catA4* and *tet(J)*, were located on a novel integrative conjugative element, designated ICEPmiChnXH1653 according to the proposed nomenclature of ICEs (14). The name of this new ICE had been registered with Adam Roberts in Liverpool, United Kingdom, as *Tn7349* (23).

Genetic structure of ICEPmiChnXH1653. ICEPmiChnXH1653 has a length of 165,609 bp (bases 2138935 to 2304493 in XH1653) and a GC content of 50.0%. It was found integrated into the 5' end of the *prfC* gene, a common insertion site for ICEs in the SXT/R391 family (Fig. 1B). ICEPmiChnXH1653 consisted of a highly conserved backbone involved in essential functions of SXT/R391 ICEs, such as integration (*int* and *xis*),

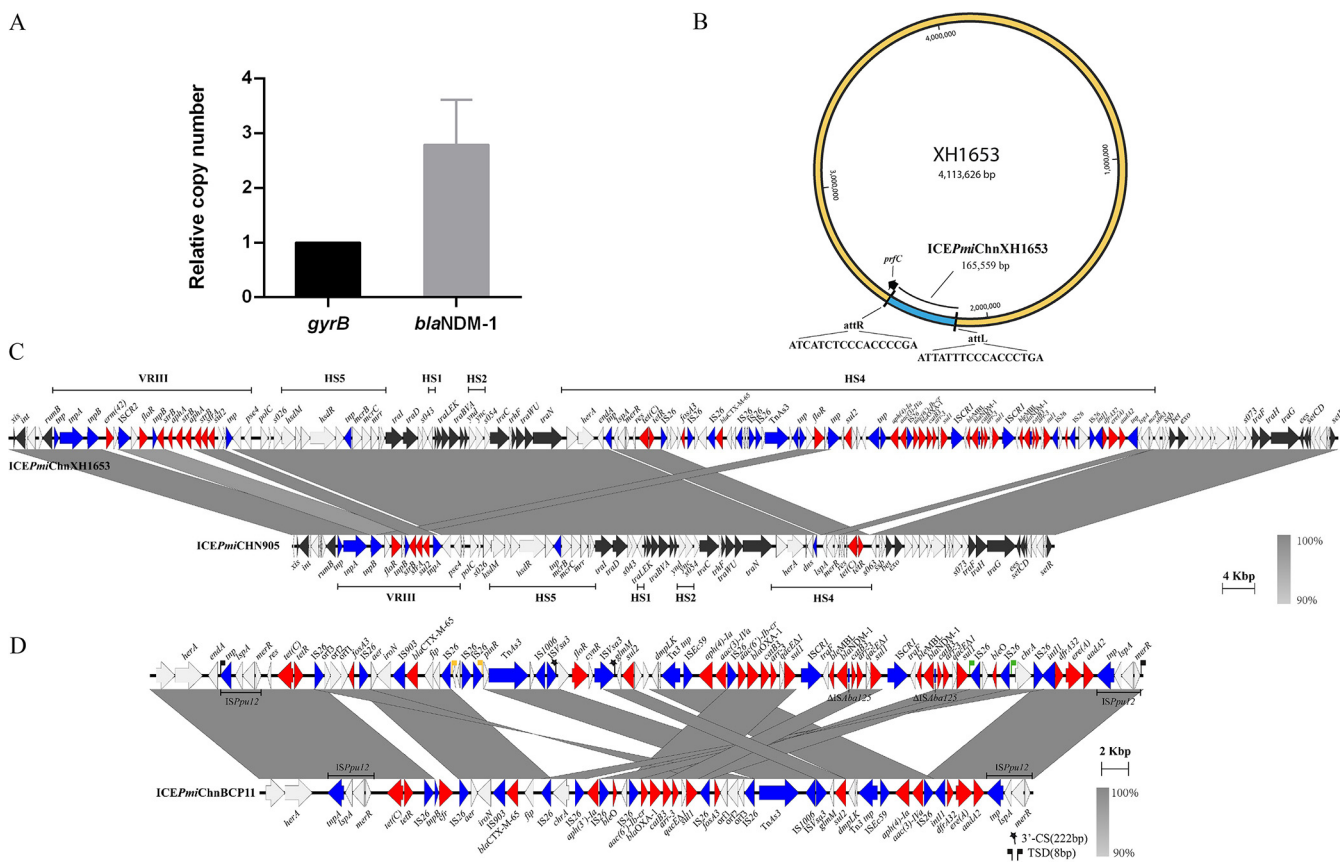


FIG 1 Characterization of *bla*_{NDM-1}-bearing *P. mirabilis* strain XH1653. (A) Relative quantification of *bla*_{NDM-1}-*gyrB* was used as control. (B) Graphical map of the XH1653 chromosome. (C and D) Genetic structure of ICEPmiChnXH1653. (C) ICEPmiChnXH1653 compared with ICEPmiChn905 (KX243412.1). (D) HS4 of ICEPmiChnXH1653 compared with HS4 of ICEPmiChnBCP11 (MG773277). ARGs are in red, transposase or integrase genes are in blue, core genes are in black, and other genes are in white. Different colors of target site duplication (TSD) in panel D represent different TSD sequences.

mating pair formation (*traLEKBVA*), exclusion determination (*traG* and *ees*), DNA recombination (*bet* and *exo*), and regulation (*setR*) (24). BLAST analysis showed that ICEPmiChnXH1653 had 100% nucleotide identity at 98% coverage to ICEPmiChn905 that was found in the *P. mirabilis* strain MD20140905 isolated from stool samples from diarrhea patients in Beijing, China, in 2014, with two region divergences in VRIII and HS4 (Fig. 1C) (25), indicating that ICEPmiChnXH1653 might have a common origin with ICEPmiChn905.

Characterization of VRIII and HS4 region of ICEPmiChnXH1653. ICEPmiChnXH1653 harbored two multidrug resistance (MDR) regions in VRIII and HS4, respectively. VRIII contained six ARGs, including *erm(42)*, *floR*, *strB* (three copies), *aphA* (two copies), *strA*, and *sul2*. Structural comparison showed that the formation of this MDR cluster in VRIII was likely due to the abundance of transposases and ISCR2 elements.

The MDR region HS4 is 73.75 kb and harbors 19 ARGs coding for β -lactam, fluoroquinolone, fosfomycin, tetracycline, aminoglycoside, sulfamethoxazole, trimethoprim, streptomycin, phenicol, rifamycin, macrolide, and bleomycin resistance, which are clustered together in an IS*Ppu12*-mediated composite transposon flanked by the 8-bp target site duplication (TSD) TAAAGAAA. According to a BLAST analysis, HS4 in ICEPmiChnXH1653 had 99.92% nucleotide identity at 82% coverage to the HS4 in ICEPmiChnBCP11 that was found in the *P. mirabilis* strain BCP11 isolated from a fecal swab of a diseased pig with diarrhea in Sichuan Province of China in November 2016, and with the exception of *cfi*, carried all the ARGs that were found in ICEPmiChnBCP11. The HS4 region of ICEPmiChnXH1653 also has a similar genetic environment as HS4 of ICEPmiChnBCP11, which suggests that these two ICES isolated from China share an IS*Ppu12*-mediated region (Fig. 1D). However, there are major differences between them: two copies of the carbapenemase gene *bla*_{NDM-1} and the

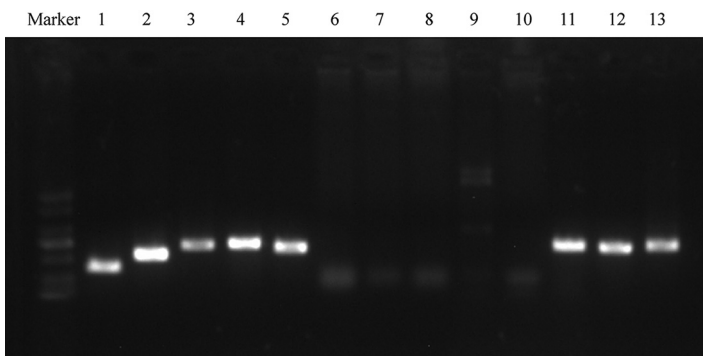
TABLE 1 Antimicrobial susceptibilities of *P. mirabilis* XH1653, *E. coli* EC600, and the transconjugants *E. coli* XH1814 and *E. coli* XH1815

Strain	MIC (mg/liter) of drug ^a :						
	MEM	IPM	GEN	FEP	CIP	TET	SXT
XH1653	16	32	32	32	64	64	>32
EC600	0.03	0.25	1	0.125	0.25	0.5	≤0.25
XH1814	8	4	32	32	0.25	32	>32
XH1815	0.015	0.25	32	8	0.5	32	>32

^aAbbreviations: MEM, meropenem; IPM, imipenem; GEN, gentamicin; FEP, cefepime; CIP, ciprofloxacin; TET, tetracycline; SXT, trimethoprim-sulfamethoxazole.

chloramphenicol ARG *floR* were detected in the HS4 region of ICEPmiChnXH1653. Further analysis of the insertion sequences surrounding *bla*_{NDM-1} revealed two tandem copies of an ISCR1 element (*ISCR1-traF-ble*_{MBL}-*bla*_{NDM-1}- Δ *ISAb125-catB3-arr-3-qacE Δ 1-sul1*). The sequence of the ISCR1 element in the HS4 region of ICEPmiChnXH1653 showed 99.95% nucleotide identity to plasmid pNDM-PM58 from *P. mirabilis* (GenBank accession no. [KP662515.1](#)). Moreover, the two tandem copies of the ISCR1 element were also seen in *Escherichia coli* Y5 (99.98% nucleotide identity; GenBank accession no. [CP013483](#)) that was reported by our lab in 2016 (26). The *floR* gene was flanked by ISVsa3 elements with a 222-bp 3'-conserved segment (3'-CS), indicating that ISVsa3 promotes the dissemination of *floR*. Two copies of IS26 adjacent to *bleO* are in the same orientation, while another IS26 and two genes (encoded recombinase family protein and transposase, respectively) lie in the opposite orientation, flanked by identical 8-bp TSDs (GTTCATAC; CGCCGGTG). This indicates that IS26 is involved in the accumulation of resistance genes and the rearrangement of multidrug resistance regions.

Transfer ability of ICEPmiChnXH1653. To test this ability to transfer ICEPmiChnXH1653, conjugation experiments were performed, with the *P. mirabilis* strain XH1653 as donor and the rifampin-resistant strain *E. coli* EC600 as recipient. ICEPmiChnXH1653 was successfully transferred to *E. coli* EC600 with a frequency of 1.5×10^{-7} transconjugants per recipient cell and chromosomally integrated into the 5' end of *prfC*. The positive transconjugant, subsequently referred to as XH1814, was confirmed by matrix-assisted laser desorption ionization–time of flight mass spectrometry (MALDI-TOF MS) and PCR detection of *int*, *attL*, *attR*, and the carbapenemase gene *bla*_{NDM-1}. Antimicrobial susceptibility testing showed XH1814 acquired resistance to all antimicrobials tested, apart from ciprofloxacin (Table 1). Excision of the ICEPmiChnXH1653 and the presence of a circular form were analyzed using PCR with primers LE4 and RE4 (24). The analysis confirmed occurrence of the circular ICE in XH1653 and XH1814 (Fig. 2), indicating that ICEPmiChnXH1653 could form circular intermediates.

**FIG 2** PCR electrophoresis map of XH1814 (lanes 1 to 5), EC600 (lanes 6 to 10), and XH1653 (lanes 11 to 13). Lanes 1 and 6 were the *attL* fragment; lanes 2 and 7 were the *attR* fragment; lanes 3, 8, and 11 were the *int* fragment; lanes 4, 9, and 12 were the *bla*_{NDM-1} fragment; lanes 5, 10, and 13 were the fragment of the circular ICE.

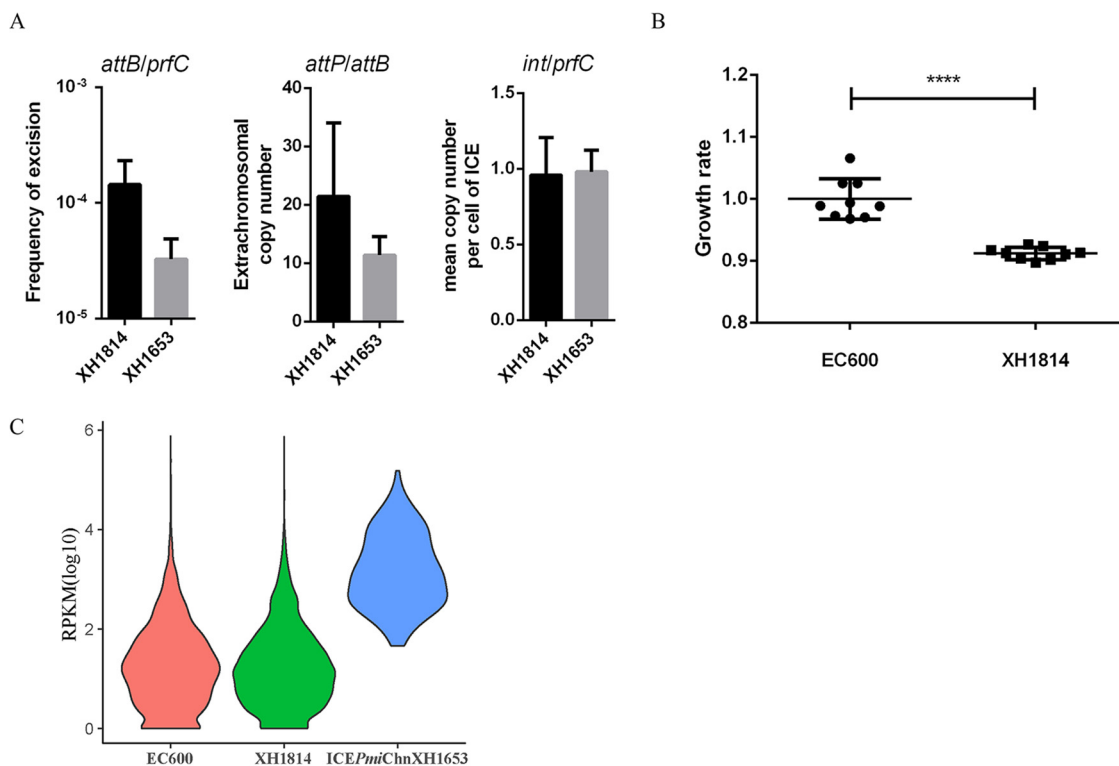


FIG 3 Characterization of the biology of ICE*PmiChn*XH1653. (A) Frequency of excision, extrachromosomal copy number of the ICE, and the mean copy number per cell of ICE*PmiChn*XH1653 in XH1814 and XH1653. (B) Growth rates of XH1814 and EC600. The experiment was repeated in triplicate. Representative results of three independent experiments are shown, and the data are the mean ± standard deviation (SD). ****, $P < 0.0001$ (Student's *t* test). (C) The gene expression value (RPKM) in EC600, XH1814 (excluding the genes in ICE*PmiChn*XH1653), and ICE*PmiChn*XH1653 in XH1814.

To investigate the biology of ICE*PmiChn*XH1653, we evaluated three dynamic factors in both the ancestor strain and the recipient strain. Real-time quantitative PCR assays were developed to determine the percentages of *int/prfC* (mean copy number per cell), *attB/attP* (extrachromosomal copy number of the ICE), and *attB/prfC* (the frequency of excision) in a culture (Fig. 3A). The ratio of *int/prfC* was found to be 0.96 ± 0.20 for XH1814 and 0.98 ± 0.11 for XH1653, as expected for a single copy of an ICE integrated in the chromosome *prfC* target. The results of *attB/attP* showed that ICE*PmiChn*XH1653 in XH1814 exhibited a relatively higher excision frequency than the ICE in XH1653; this might indicate that the ICE is not as stable in *E. coli* as it is in the original host. We also found that both XH1814 and XH1653 had multiple copies of extrachromosomal ICEs (21 ± 10 and 11 ± 3 , respectively), suggesting that the circular intermediate of ICE*PmiChn*XH1653 is capable of replicating in a small subset of the cell population.

Presence of ICE*PmiChn*XH1653 influences host fitness and transcriptome. To estimate the fitness cost of ICE carriage, we compared growth rates of the transconjugant XH1814 and the ICE-free recipient strain EC600 in Mueller-Hinton (MH) liquid medium. XH1814 containing ICE*PmiChn*XH1653 exhibited a significantly decreased growth rate compared to the strain without the ICE, EC600 (Fig. 3B), indicating that ICE*PmiChn*XH1653 confers a fitness cost on the host.

To better understand the molecular basis for the decrease in fitness due to ICE*PmiChn*XH1653 in EC600, we performed transcriptomic analyses of the strain with and without the ICE (XH1814 versus EC600) using RNA sequencing (RNA-Seq). In comparison to strain EC600, a total of 22 genes were differentially expressed in XH1814 (false-discovery rate [FDR] < 0.05). Among them, nine genes were upregulated, and 13 genes were downregulated (see Table S1 in the supplemental material). The upregulated genes were involved in lipid metabolism and amino acid metabolism, and the downregulated genes

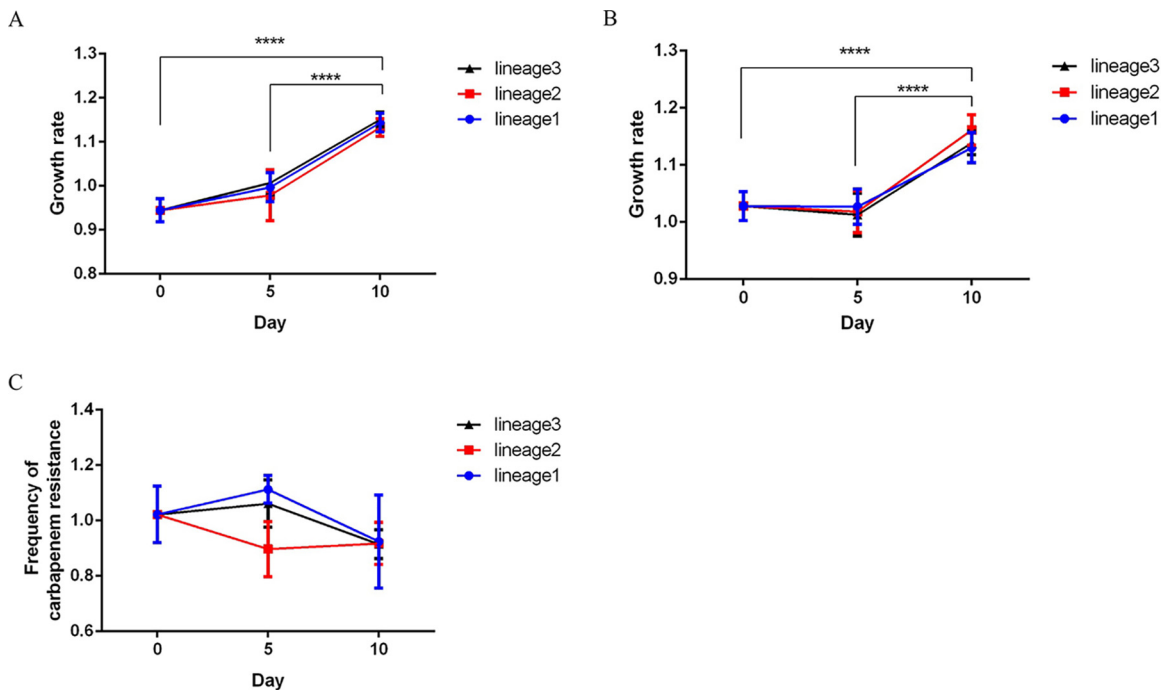


FIG 4 Characterization of the evolution of ICEPmiChnXH1653. (A and B) Line charts of experimental evolution of XH1814 (A) and EC600 (B) in MH broth without antibiotics. (C) Line chart of the frequency of XH1814 harboring the carbapenem resistance. The data represent the averages from three experiments. Standard errors of the means are indicated. The P values represent the averages from three lineages and were determined by two-tailed Student's t tests. ****, $P < 0.0001$.

were involved in the metabolic pathway, replication and repair pathway, and quorum sensing pathway. Increased transcription of genes encoding 4-oxalomesaconate tautomerase (DK885_16125), bifunctional aldehyde dehydrogenase (DK885_12690), hydrogenase-4 component J (DK885_06720), and galactose-proton symporter (DK885_04375) was noticeable, whereas genes for multidrug resistance protein (MdtL), guanine/hypoxanthine permease (GhxQ), and cold shock protein (CspB) were expressed at lower levels in XH1814. We also compared gene expression levels of EC600 and XH1814 using the average reads per kilobase per million mapped reads (RPKM), with no significant difference between the detectable levels. However, the average RPKM of ICE in XH1814 was higher than the average RPKM of EC600 or XH1814 ($P < 0.05$) (Fig. 3C).

XH1814 lost carbapenem resistance following repeated laboratory passage.

Given the apparent cost of the ICEPmiChnXH1653 carriage, we performed experimental evolution experiments with the transconjugant XH1814 and the ICE-free recipient strain EC600 as a control to identify the putative emergence of compensatory mechanisms associated with ICE carriage. We observed that the strain on day 10, "XH1814D10," had a significantly faster growth than XH1814 and the strain on day 5 (Fig. 4A). However, the ICE-free control strain also showed evolutionary adaptations with significantly faster growth than the strain on day 0 and day 5 (Fig. 4B). As compensatory mutations may not be associated with ICE carriage, we chose not to trace compensatory mutations on the whole-genome level. When testing the presence of ICEPmiChnXH1653 in "XH1814D10" using PCR with *bla*_{NDM-1} primers, we observed that the *bla*_{NDM-1} gene was lost while still retaining the ICE (Fig. 5A and B). This strain, named XH1815, had become susceptible to imipenem and meropenem (Table 1). Also, the loss of carbapenem resistance was observed, albeit at a low frequency (8.14% of the colonies) (Fig. 4C).

ISCR1 and ISVs α 3 elements were deleted in XH1815. The whole genome of XH1815 was sequenced at high accuracy in order to analyze the molecular events that resulted in the deletion of *bla*_{NDM-1}. Strain XH1815 was found to harbor the ICE with a size of 148,447 bp, subsequently referred to as ICEPmiChnXH1815, which chromosomally integrated into the 5' end of the *prfC* gene. Comparative analysis

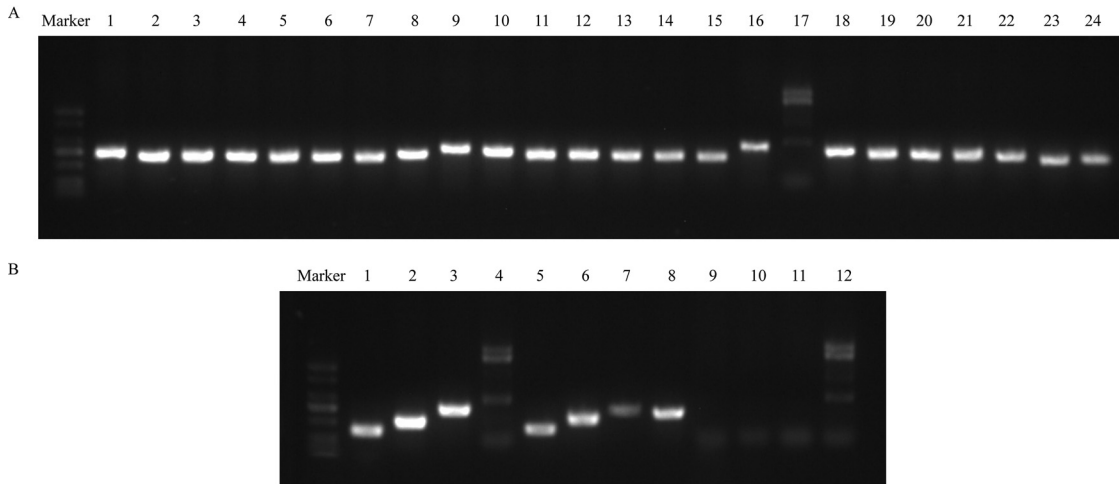


FIG 5 PCR electrophoresis map. (A) Detecting the *bla*_{NDM-1} fragment of XH1814D10. (B) Detecting the *attL*, *attR*, *int*, and *bla*_{NDM-1} fragments of XH1815 (lanes 1 to 4), XH1814 (lanes 5 to 8), and EC600 (lanes 9 to 12). Lanes 1, 5, and 9 were the *attL* fragment; lanes 2, 6, and 10 were the *attR* fragment; lanes 3, 7, and 11 were the *int* fragment; lanes 4, 8, and 12 were the *bla*_{NDM-1} fragment.

showed ICEPmiChnXH1815 to exhibit sequence coverage of 99% and identity of 100% to ICEPmiChnXH1653. A deletion of two fragments was found in the HS4 region of ICEPmiChnXH1815 (Fig. 6A) and corresponds to the tandem copies of the ISCR1 and ISVsa3 elements that included the carbapenemase gene *bla*_{NDM-1} and the chloramphenicol ARG *floR*, respectively (Fig. 6B). Our results indicate that ICEPmiChnXH1653 obtained the carbapenemase gene by ISCR1-mediated homologous recombination. As observed in ICEPmiChnXH1815, only one copy of the ISVsa3 was found, and the ISVsa3 element (*hp-floR-cynR-ISVsa3*) was deleted compared to ICEPmiChnXH1653. We also detected the circular intermediate of the ISVsa3 element, which suggests that ISVsa3-mediated transfer of *folR* had occurred and the circular intermediate *hp-floR-cynR-ISVsa3* had inserted at the location of ISVsa3.

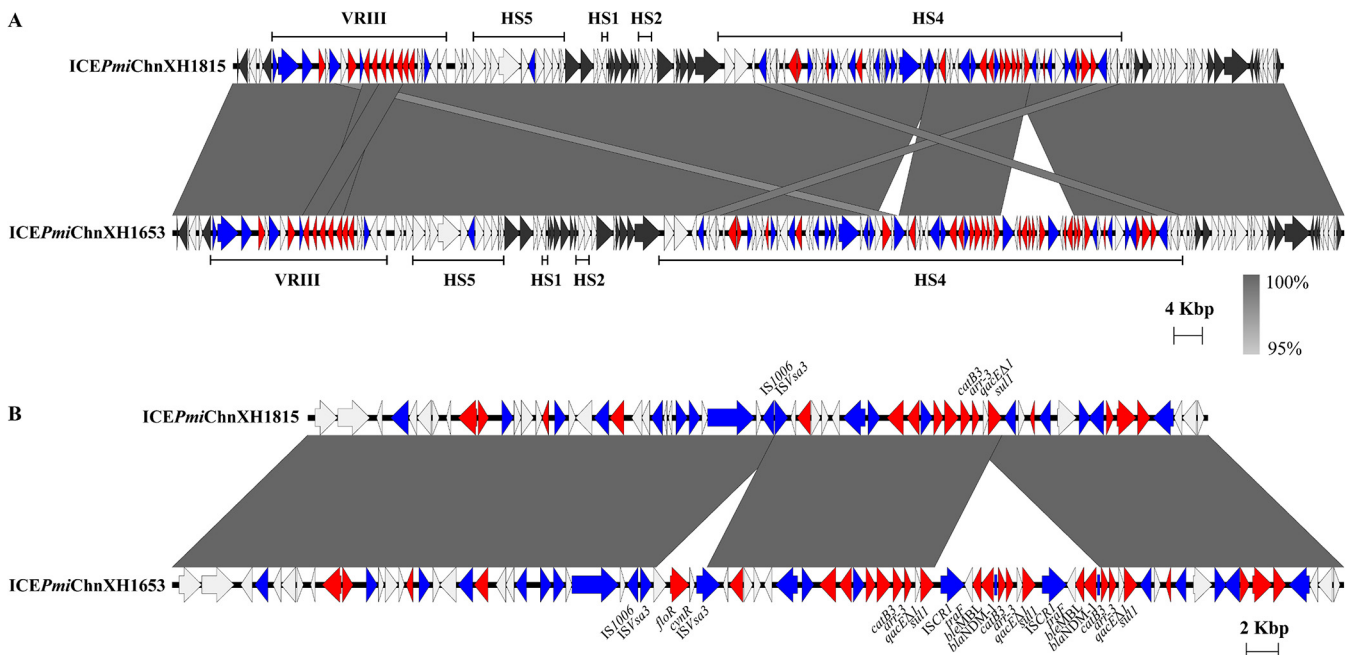


FIG 6 Genetic structure of ICEPmiChnXH1815. (A) ICEPmiChnXH1815 compared with ICEPmiChnXH1653. (B) HS4 of ICEPmiChnXH1815 compared with HS4 of ICEPmiChnXH1653. ARGs are in red, transposase or integrase genes are in blue, core genes are in black, and other genes are in white.

DISCUSSION

The observed increase of *P. mirabilis* strains that are resistant to carbapenem mediated by the *bla*_{NDM-1} gene is of concern as only a limited number of antimicrobials remain available for clinical therapy (12). In this study, we isolated an XDR *P. mirabilis* strain, XH1653, from a patient suffering from a urinary tract infection, which was resistant to all tested antibiotics with the exception of aztreonam. qPCR and sequencing analysis showed that XH1653 carried two copies of *bla*_{NDM-1}, which are located in a so-far-undescribed SXT/R391 ICE.

Mobile elements are associated with the formation of clusters containing ARGs in which different determinants that lead to the MDR phenotype are found in close genetic proximity (27). Antimicrobial resistance determinants in ICE*PmiChn*XH1653 are carried within VRIII and HS4 regions that are integrated within the conserved ICE backbone, and most of them are located within ARG arrays, composed of ARGs or clusters thereof, and mobile genetic elements such as IS elements, transposons, or integrons. The genes *floR*, *strB*, *strA*, and *sul2* are frequently found in the VRIII region of SXT/R391 ICE members (28). Also, *erm(42)* and *aphA* are observed in the VRIII region of ICE*AplChn1* in *Actinobacillus pleuropneumoniae* (29). Our finding is also the first report of two copies of the resistance gene fragment *strB-aphA* in VRIII.

The *bla*_{NDM-1} gene is mainly and widely spread by an IS*Aba125*-bounded composite transposon Tn125 (9), which is often located on plasmids in *Enterobacteriaceae* (12, 30, 31). Recently, Kong et al. reported that *bla*_{NDM-1} was embedded in a truncated IS*Aba125* composite transposon flanked by IS26 in the ICE from *P. vulgaris* (13). However, the genetic environment around *bla*_{NDM-1} in ICE*PmiChn*XH1653 is different from the ICE in the study by Kong et al., which revealed two tandem copies of an ISCR1 element. A 151-bp truncated IS*Aba125* is found upstream of *bla*_{NDM-1}, while the ISCR1 lies downstream of both copies of the *bla*_{NDM-1} gene and is followed by the bleomycin ARG *ble*_{MBL} and the *trpF* gene, which are often identified near *bla*_{NDM-1} (9). The ISCR1-like elements might be responsible for the mobilization of *bla*_{NDM-1} via the rolling-circle replication in *Enterobacteriaceae* (30, 32, 33). In our study, we also observed that the two tandem copies of the ISCR1 element (ISCR1-*traF-ble*_{MBL}-*bla*_{NDM-1}- Δ IS*Aba125-catB3-arr3-qacE Δ 1-sul1*) were lost following extended passage under nonselective conditions, which is a clear indication that two tandem copies of the ISCR1 element move into the 3'-CS (*qacE Δ 1/sul1*) of a class 1 integron [*aac(6')*-*lb-cr-bla*_{OXA-1}-*catB3-arr3-qacE Δ 1-sul1*] by homologous recombination, resulting in the transmission of *bla*_{NDM-1}. Homologous recombination is likely to contribute extensively to the duplication of ARGs when no selective pressure is applied. It is possible that the a single ISCR1 element mobilizes the *bla*_{NDM-1} gene to move into the 3'-CS by rolling-circle transposition and that after attachment, subsequent homologous recombination may result in a duplication of the ARG (34). A similar structure of the two tandem copies of the ISCR1 element was also observed in the chromosome of *E. coli* Y5 (GenBank accession no. CP013483) (26), and one copy of the ISCR1 element appears to be intact in the plasmid from *P. mirabilis* (GenBank accession no. KP662515), suggesting a potential translocation of the *bla*_{NDM-1} gene between different mobile genetic elements (ICEs and plasmids) and the integration into the chromosome. To the best of our knowledge, this is the first description of two copies of *bla*_{NDM-1} embedded within the ISCR1 element, not only in the SXT/R391 element but also in *P. mirabilis*. IS*Vsa3* belongs to the ISCR2 family; two copies of the IS*Vsa3* in the same orientation were found in the HS4 region of ICE*PmiChn*XH1653, which contained the chloramphenicol ARG *floR*. He et al. reported that IS*Vsa3* is able to mediate the transposition of *tet(X)*-carrying cassettes and that the circular intermediate was able to insert at the location of IS*Vsa3* on the plasmid (35). We found that the IS*Vsa3* element (*hp-floR-cynR-ISVsa3*) was lost during the serial passage in the laboratory, indicating the IS*Vsa3*-mediated transfer of *floR* had occurred and ISCR elements played a major role for the host bacteria in the mobilization and accumulation of antibiotic resistance genes. After the deletion of the ISCR1 and IS*Vsa3* element in ICE*PmiChn*XH1653, the HS4 of the ICE exhibited a high similarity to the HS4 of ICE*PmiBCP11* with a coverage of

TABLE 2 Bacterial strains used in this study

Strain	Description
XH1653	ICEPmiChnXH1653-carrying multidrug-resistant <i>P. mirabilis</i> , wild-type strain
XH1814	ICEPmiChnXH1653-carrying transconjugant, EC600 as the recipient strain
XH1815	Selected isolate of XH1814D10, containing ICEPmiChnXH1815
EC600	ICE-free recipient strain, rifampin resistance
EC600D5	EC600 population at the 5th day of passage
EC600D10	EC600 population at the 10th day of passage
XH1814D5	XH1814 population at the 5th day of passage
XH1814D10	XH1814 population at the 10th day of passage

95% (increase from 82% to 95%) and a sequence identity of 99.95%, contributing to our knowledge of how the dissemination of an *IS**Ppu12*-mediated composite MDR transposon in different *P. mirabilis* strains occurs. A general observation is that the ICEPmiChnXH1653 has been highly efficient in recruiting antimicrobial resistance traits. It has been suggested that recent MDR members of the SXT/R391 family could have evolved from a common ancestor through stepwise integration of horizontally acquired ARG arrays into the conserved backbone.

Here, we performed an integrative approach to gain insights into different aspects of ICEPmiChnXH1653 evolution and biology. An intergenus transfer of ICEPmiChnXH1653 from *P. mirabilis* to *E. coli* EC600 at a frequency of 1.5×10^{-7} was observed, which is relatively low for SXT/R391 (22). The ICEPmiChnXH1653 in the recipient strain exhibited a higher excision frequency and extrachromosomal copy number than the ICE in the ancestor strain. As expected for one *attP* site on the circular ICE resulting in one unoccupied *attB* site on the chromosome (*attP/attB* = 1), an increase in the copy number of *attP/attB* would indicate that the excised ICE replicates more frequently than the chromosome (36). The extrachromosomal autonomous replication appears to be common for ICEs, as our results for *attP/attB* were consistent with previous reports (36, 37). The relatively higher excision frequency in recipient strain EC600 may be caused by a genetic instability after entering a new host cell. We also found that the acquisition of ICEPmiChnXH1653 results in a fitness cost for the ICE-free recipient strain EC600. Here, several genes showed altered transcription in EC600 after the acquisition of ICE. This number was lower than a report which described that a total of 161 genes were differentially expressed in *Pseudomonas putida* with the ICE*clc* (38). The presence of the ICE*clc* can influence a number of cellular pathways, resulting in direct benefits but also in indirect costs for *P. putida* (38). The difference of the impact on the transcription of the bacteria might be caused by the genetic interrelationship of the strains used in the studies: the original host of ICE*clc* is *Pseudomonas knackmussii* B13, with the new host in the study by Miyazaki et al. (38) belonging to the same genus. However, in our project we used EC600 as the new host for the *P. mirabilis* XH1653-derived element ICEPmiChnXH1653. Interestingly, the genes carried in ICEPmiChnXH1653 showed a higher expression in XH1814 compared to the average expression in EC600 or XH1814, confirming ICEPmiChnXH1653 activation in XH1814, possibly explaining the burden in fitness.

In conclusion, this is the first report of a novel SXT/R391 ICE carrying two tandem copies of *bla*_{NDM-1}. The genetic environment of *bla*_{NDM-1} was identical to that of the previously reported *bla*_{NDM-1}-carrying plasmid of *P. mirabilis* PM58 and chromosome of *E. coli* Y5. The ICEPmiChnXH1653 could be transferred between bacterial genera—within the order *Enterobacteriales*—from *P. mirabilis* to *E. coli*, indicating that the transmission of *bla*_{NDM-1} by ISCR1 elements or ICEs may be an important contributor to the carbapenem resistance development across species.

MATERIALS AND METHODS

Bacterial strains and susceptibility testing. *P. mirabilis* strain XH1653 was isolated in October 2015 from a urine sample of a 49-year-old male patient in a hospital in Zhejiang province, China. All isolates used in this study (Table 2) were cultured in MH agar plates or broth (Oxoid, Hampshire, United Kingdom) and Luria-Bertani (LB) broth (Sangon Biotech, Shanghai, China) at 37°C. The following 21

TABLE 3 Primers used in this study

Target	Primer	Primer sequence (5'–3')	Amplicon size (bp)
<i>attL</i>	C600-LE-1	GTTTCTTCGTTGCACGAACTGG	348
	LE-4	GTACACACTTTCCGAGGTTACG	
<i>attR</i>	C600-RE-1	CGGTCTGAATGGCCTGTCCGAA	464
	RE-4	CCGCAATACCCTGCAATACCGA	
<i>int</i>	ICE-int-F	CGTAACCTCGGAAAGTGTGTAC	640
	ICE-int-R	TGTGCCACAGCTTGTTCGTG	
<i>bla_{NDM-1}</i>	NDM-1-F	TTGCCCAATATTATGCACCC	552
	NDM-1-R	GCCGGGGTAAAATACCTTGA	
<i>bla_{NDM-1}</i> (for qPCR)	QNDM-1-F	AACGCATTGGCATAAGTCGC	178
	QNDM-1-R	GATACCGCCTGGACCGATG	
<i>gyrB</i> (for qPCR)	QgyrB-F	GACGCCACCAGAGACTTTA	192
	QgyrB-R	TCGCGGGTTACTGTGATGAG	
<i>attB</i> of EC600 (for qPCR)	QC600-attB-F	CGACTTAGCGTGTGGTTGG	201
	QC600-attB-R	GCGATGCCGCTTACTCAAGA	
<i>attB</i> of XH1653 (for qPCR)	Q1653-attB-F	AGTGCAGTGCATTCACTTGTT	198
	Q1653-attB-R	TTGAGCCACGCCCTTTACT	
<i>prfC</i> of EC600 (for qPCR)	QC600-prfC-F	GTCACCCGCCATAAAGGTCA	194
	QC600-prfC-R	CCGTAGAAGCGAGCGAAGAT	
<i>prfC</i> of XH1653 (for qPCR)	Q1653-prfC-F	TGGCCTGCATAATCACGGTA	190
	Q1653-prfC-R	AAACACCTGTACCGCACCTT	
<i>attP</i> (for qPCR)	QICE-attP-F	AACACGACGGATTTGACAAGC	221
	QICE-attP-R	ACGTAGAGATGTGATTGTGGTGT	
<i>int</i> (for qPCR)	QICE-int-F	TATACGACGCTCTGGCGAAG	192
	QICE-int-R	AAACCATCATCGAGCCGACA	

compounds were tested using the BD Phoenix 100 automated microbiology system (Becton, Dickinson, MD, USA): imipenem, meropenem, gentamicin, amikacin, cefazolin, ceftazidime, cefotaxime, cefepime, ampicillin, piperacillin, amoxicillin-clavulanate, ampicillin-sulbactam, piperacillin-tazobactam, trimethoprim-sulfamethoxazole, ciprofloxacin, chloramphenicol, levofloxacin, moxifloxacin, aztreonam, tetracycline, and colistin. Susceptibility of XH1653, EC600, XH1814, and XH1815 to antibiotics (imipenem, meropenem, gentamicin, cefepime, ciprofloxacin, tetracycline, and trimethoprim-sulfamethoxazole) was also determined by the broth microdilution method. The results of susceptibility testing were interpreted according to the Clinical and Laboratory Standards Institute (CLSI) guidelines (39). *E. coli* ATCC 25922 served as a control strain.

Whole-genome sequencing and sequence analysis. Genomic DNA was extracted and subjected to whole-genome sequencing using both the Illumina HiSeq and Nanopore MinION platforms at Zhejiang Tianke (Hangzhou, China). Long-read library preparation for Nanopore sequencing was performed with a one-dimensional (1D) sequencing kit (SQK-LSK109; Nanopore). The libraries were sequenced on a MinION device with a 1D flow cell (FLO-MIN106; Nanopore) and base called with Guppy v2.3.5 (Nanopore). Long- and short-read sequence data were used in a hybrid *de novo* assembly using Unicycler v0.4.8 (40), followed by Pilon v1.23 (41). ARGs were identified using the ResFinder database (42) with Abricate 0.8 (<https://github.com/tseemann/abricate>). The complete nucleotide sequence of ICE in the strain XH1653 was identified by ICEfinder (<https://db-mml.sjtu.edu.cn/ICEfinder/>) with manual modification (43). Sequence comparisons were performed using BLASTn v2.4.0 (44) and visualized using Easyfig v2.2.3 (45).

Bacterial conjugations. Conjugation experiments were carried out by filter mating with the rifampin-resistant *E. coli* EC600 as recipient. Overnight cultures of XH1653 and EC600 were mixed on an MH plate and incubated at 37°C for 18 h. The cells on the membrane were collected, resuspended in saline solution, and serially diluted before plating. Donors, recipients, and transconjugants were selected on MH agar plates containing 100 mg/liter rifampin and 100 mg/liter ampicillin. The successful transconjugants were identified by MALDI-TOF MS (bioMérieux, France), and the presence of *bla_{NDM-1}*, *attL*, *int*, and *attR* as the marker sequences of ICE in transconjugants was determined by PCR (Table 3). The MIC profiles of the transconjugants were determined for differentiation between transconjugants and donor strains. The transconjugant was designated XH1814. The ICE transfer frequency was calculated as the number of transconjugants per donor cell.

Growth rate determination. Three independent cultures of EC600 and XH1814 were grown overnight and diluted to 1:100 in MH broth, and then aliquots were placed into a flat-bottom 100-well plate in three replicates. The plate was incubated at 37°C with agitation. The optical density at 600 nm (OD_{600}) of each culture was continuously determined for 20 h using a Bioscreen C MBR machine (Oy Growth Curves Ab Ltd., Finland). Growth rate was estimated based on OD_{600} curves using an R script as previously described (46), and values returning a *P* value of <0.05 from a Student *t* test were taken as significant.

Real-time quantitative PCR. The frequency of excision and mean copy number per cell, extrachromosomal copy number of the ICE, and the copy number of *bla_{NDM-1}* per chromosome were assessed by real-time quantitative PCR (37), using the formula as described previously (47). The genomic DNA was extracted using the QIAamp DNA minikit (Qiagen, USA), and quality and quantity of genomic DNA were

determined by a NanoDrop spectrophotometer. Primers are listed in Table 3. Triplicate samples were included in each run, and qPCR experiments were performed in triplicate using TB Green Premix *Ex Taq* II (TaKaRa Bio) in a LightCycler 480 system (Roche, Switzerland).

RNA-Seq. Three single colonies of EC600 and XH1814 were cultured overnight at 37°C in MH broth. Strains were diluted 1:100 in 100 ml of fresh MH broth and harvested at the mid-log growth phase. The cells were collected at 4°C using centrifugation (5,000 rpm, 10 min). Total RNA was extracted using TRIzol reagent (Invitrogen, Carlsbad, CA, USA) after liquid nitrogen grinding. Bacterial mRNA sequence library construction and sequencing were performed by Zhejiang Tianke (Hangzhou, China) (48). The sequenced reads were mapped to the EC600 genome and ICE sequence, respectively, using Rockhopper version 2.0.3 (49). The raw read count in output of Rockhopper was analyzed by the edgeR package (50). ggplot2 was used for figure generation (51).

Experimental evolution under nonselective conditions. Three single colonies of XH1814 and the EC600 ancestor strain were inoculated in MH broth without antibiotics and cultured under shaking (200 rpm) at 37°C. All evolved lineages were passaged daily. A 20- μ l volume of overnight culture was collected and used for inoculation at a 1:100 dilution every day. Growth curves were performed every 5 days to assess the evolutionary changes.

Detection of carbapenem resistance loss. XH1814, three lineages of XH1814 at day 5, and three lineages of XH1814 at day 10 were incubated in MH broth at 37°C for 18 h. Overnight cultures were serially diluted before plating and were selected on an MH agar plate without antibiotics or with 0.25 mg/liter meropenem, respectively. The frequency of carbapenem resistance in XH1814 was calculated as the number of cells observed on an MH agar plate containing 0.25 mg/liter meropenem versus cells observed on an MH agar plate without antibiotics. The detection experiments were performed in triplicate.

Data availability. The complete genome sequences of *P. mirabilis* XH1653 and *E. coli* XH1815 isolates were deposited in GenBank under accession numbers CP065039 and CP069386, respectively. The RNA-Seq data from *E. coli* EC600 and *E. coli* XH1814 were deposited in GenBank under BioProject no. PRJNA699923.

SUPPLEMENTAL MATERIAL

Supplemental material is available online only.

TABLE S1, PDF file, 0.1 MB.

ACKNOWLEDGMENTS

This work was supported by grants from the National Key Research and Development Program of China (2018YFE0102100) and the Zhejiang Provincial Medical and Health Science and Technology Plan (2018KY635).

There are no competing interests to declare.

REFERENCES

- Schaffer JN, Pearson MM. 2015. *Proteus mirabilis* and urinary tract infections. *Microbiol Spectr* 3:10.1128/microbiolspec.UTI-0017-2013. <https://doi.org/10.1128/microbiolspec.UTI-0017-2013>.
- Kanzari L, Ferjani S, Saidani M, Hamzaoui Z, Jendoubi A, Harbaoui S, Ferjani A, Rehaïem A, Boutiba Ben Boubaker I, Slim A. 2018. First report of extensively-drug-resistant *Proteus mirabilis* isolate carrying plasmid-mediated blaNDM-1 in a Tunisian intensive care unit. *Int J Antimicrob Agents* 52:906–909. <https://doi.org/10.1016/j.ijantimicag.2018.06.009>.
- Yong D, Toleman MA, Giske CG, Cho HS, Sundman K, Lee K, Walsh TR. 2009. Characterization of a new metallo-beta-lactamase gene, bla(NDM-1), and a novel erythromycin esterase gene carried on a unique genetic structure in *Klebsiella pneumoniae* sequence type 14 from India. *Antimicrob Agents Chemother* 53:5046–5054. <https://doi.org/10.1128/AAC.00774-09>.
- Nordmann P, Poirel L, Walsh TR, Livermore DM. 2011. The emerging NDM carbapenemases. *Trends Microbiol* 19:588–595. <https://doi.org/10.1016/j.tim.2011.09.005>.
- Dortet L, Poirel L, Nordmann P. 2014. Worldwide dissemination of the NDM-type carbapenemases in Gram-negative bacteria. *Biomed Res Int* 2014:249856. <https://doi.org/10.1155/2014/249856>.
- Walsh TR, Weeks J, Livermore DM, Toleman MA. 2011. Dissemination of NDM-1 positive bacteria in the New Delhi environment and its implications for human health: an environmental point prevalence study. *Lancet Infect Dis* 11:355–362. [https://doi.org/10.1016/S1473-3099\(11\)70059-7](https://doi.org/10.1016/S1473-3099(11)70059-7).
- Toleman MA, Spencer J, Jones L, Walsh TR. 2012. blaNDM-1 is a chimera likely constructed in *Acinetobacter baumannii*. *Antimicrob Agents Chemother* 56:2773–2776. <https://doi.org/10.1128/AAC.06297-11>.
- Loh B, Chen J, Manohar P, Yu Y, Hua X, Leptihn S. 2020. A biological inventory of prophages in *A. baumannii* genomes reveal distinct distributions in classes, length, and genomic positions. *Front Microbiol* 11:579802. <https://doi.org/10.3389/fmicb.2020.579802>.
- Wu W, Feng Y, Tang G, Qiao F, McNally A, Zong Z. 2019. NDM metallo-beta-lactamases and their bacterial producers in health care settings. *Clin Microbiol Rev* 32:e00115-18. <https://doi.org/10.1128/CMR.00115-18>.
- Partridge SR, Iredell JR. 2012. Genetic contexts of blaNDM-1. *Antimicrob Agents Chemother* 56:6065–6067. (Letter.) (Reply, 56:6071.) <https://doi.org/10.1128/AAC.00117-12>.
- Wailan AM, Paterson DL, Kennedy K, Ingram PR, Bursle E, Sidjabat HE. 2016. Genomic characteristics of NDM-producing Enterobacteriaceae isolates in Australia and their blaNDM genetic contexts. *Antimicrob Agents Chemother* 60:136–141. <https://doi.org/10.1128/AAC.01243-15>.
- Dong D, Li M, Liu Z, Feng J, Jia N, Zhao H, Zhao B, Zhou T, Zhang X, Tong Y, Zhu Y. 2019. Characterization of a NDM-1-encoding plasmid pHFk418-NDM from a clinical *Proteus mirabilis* isolate harboring two novel transposons, Tn6624 and Tn6625. *Front Microbiol* 10:2030. <https://doi.org/10.3389/fmicb.2019.02030>.
- Kong LH, Xiang R, Wang YL, Wu SK, Lei CW, Kang ZZ, Chen YP, Ye XL, Lai Y, Wang HN. 2020. Integration of the blaNDM-1 carbapenemase gene into a novel SXT/R391 integrative and conjugative element in *Proteus vulgaris*. *J Antimicrob Chemother* 75:1439–1442. <https://doi.org/10.1093/jac/dkaa068>.
- Johnson CM, Grossman AD. 2015. Integrative and conjugative elements (ICEs): what they do and how they work. *Annu Rev Genet* 49:577–601. <https://doi.org/10.1146/annurev-genet-112414-055018>.
- Burrus V, Waldor MK. 2004. Shaping bacterial genomes with integrative and conjugative elements. *Res Microbiol* 155:376–386. <https://doi.org/10.1016/j.resmic.2004.01.012>.
- Burrus V, Marrero J, Waldor MK. 2006. The current ICE age: biology and evolution of SXT-related integrating conjugative elements. *Plasmid* 55:173–183. <https://doi.org/10.1016/j.plasmid.2006.01.001>.

17. Wozniak RA, Fouts DE, Spagnoletti M, Colombo MM, Ceccarelli D, Garriss G, Dery C, Burrus V, Waldor MK. 2009. Comparative ICE genomics: insights into the evolution of the SXT/R391 family of ICEs. *PLoS Genet* 5:e1000786. <https://doi.org/10.1371/journal.pgen.1000786>.
18. Lei CW, Chen YP, Kang ZZ, Kong LH, Wang HN. 2018. Characterization of a novel SXT/R391 integrative and conjugative element carrying cfr, blaCTX-M-65, fosA3, and aac(6)-Ib-cr in *Proteus mirabilis*. *Antimicrob Agents Chemother* 62:e00849-18. <https://doi.org/10.1128/AAC.00849-18>.
19. Harada S, Ishii Y, Saga T, Tateda K, Yamaguchi K. 2010. Chromosomally encoded blaCMY-2 located on a novel SXT/R391-related integrating conjugative element in a *Proteus mirabilis* clinical isolate. *Antimicrob Agents Chemother* 54:3545–3550. <https://doi.org/10.1128/AAC.00111-10>.
20. Aberkane S, Compain F, Decre D, Dupont C, Laurens C, Vittecoq M, Pantel A, Solassol J, Carriere C, Renaud F, Brieu N, Lavigne JP, Bouzini N, Ouedraogo AS, Jean-Pierre H, Godreuil S. 2016. High prevalence of SXT/R391-related integrative and conjugative elements carrying blaCMY-2 in *Proteus mirabilis* isolates from gulls in the south of France. *Antimicrob Agents Chemother* 60:1148–1152. <https://doi.org/10.1128/AAC.01654-15>.
21. Lei CW, Zhang AY, Wang HN, Liu BH, Yang LQ, Yang YQ. 2016. Characterization of SXT/R391 integrative and conjugative elements in *Proteus mirabilis* isolates from food-producing animals in China. *Antimicrob Agents Chemother* 60:1935–1938. <https://doi.org/10.1128/AAC.02852-15>.
22. Botelho J, Schulenburg H. 2021. The Role of integrative and conjugative elements in antibiotic resistance evolution. *Trends Microbiol* 29:8–18. <https://doi.org/10.1016/j.tim.2020.05.011>.
23. Tansirichaiya S, Rahman MA, Roberts AP. 2019. The Transposon Registry. *Mob DNA* 10:40. <https://doi.org/10.1186/s13100-019-0182-3>.
24. McGrath BM, O'Halloran JA, Piterina AV, Pembroke JT. 2006. Molecular tools to detect the IncI elements: a family of integrating, antibiotic resistant mobile genetic elements. *J Microbiol Methods* 66:32–42. <https://doi.org/10.1016/j.mimet.2005.10.004>.
25. Li X, Du Y, Du P, Dai H, Fang Y, Li Z, Lv N, Zhu B, Kan B, Wang D. 2016. SXT/R391 integrative and conjugative elements in *Proteus* species reveal abundant genetic diversity and multidrug resistance. *Sci Rep* 6:37372. <https://doi.org/10.1038/srep37372>.
26. Shen P, Yi M, Fu Y, Ruan Z, Du X, Yu Y, Xie X. 2017. Detection of an *Escherichia coli* sequence type 167 strain with two tandem copies of blaNDM-1 in the chromosome. *J Clin Microbiol* 55:199–205. <https://doi.org/10.1128/JCM.01581-16>.
27. He S, Hickman AB, Varani AM, Siguier P, Chandler M, Dekker JP, Dyda F. 2015. Insertion sequence IS26 reorganizes plasmids in clinically isolated multidrug-resistant bacteria by replicative transposition. *mBio* 6:e00762-15. <https://doi.org/10.1128/mBio.00762-15>.
28. Wozniak RA, Waldor MK. 2009. A toxin-antitoxin system promotes the maintenance of an integrative conjugative element. *PLoS Genet* 5:e1000439. <https://doi.org/10.1371/journal.pgen.1000439>.
29. Xu J, Jia H, Cui G, Tong H, Wei J, Shao D, Liu K, Qiu Y, Li B, Ma Z. 2018. ICE-AplChn1, a novel SXT/R391 integrative conjugative element (ICE), carrying multiple antibiotic resistance genes in *Actinobacillus pleuropneumoniae*. *Vet Microbiol* 220:18–23. <https://doi.org/10.1016/j.vetmic.2018.05.002>.
30. Qin S, Qi H, Zhang Q, Zhao D, Liu ZZ, Tian H, Xu L, Xu H, Zhou M, Feng X, Liu HM. 2015. Emergence of extensively drug-resistant *Proteus mirabilis* harboring a conjugative NDM-1 plasmid and a novel *Salmonella* genomic island 1 variant, SGI1-Z. *Antimicrob Agents Chemother* 59:6601–6604. <https://doi.org/10.1128/AAC.00292-15>.
31. Poirel L, Dortet L, Bernabeu S, Nordmann P. 2011. Genetic features of blaNDM-1-positive Enterobacteriaceae. *Antimicrob Agents Chemother* 55:5403–5407. <https://doi.org/10.1128/AAC.00585-11>.
32. Chen CJ, Wu TL, Lu PL, Chen YT, Fung CP, Chuang YC, Lin JC, Siu LK. 2014. Closely related NDM-1-encoding plasmids from *Escherichia coli* and *Klebsiella pneumoniae* in Taiwan. *PLoS One* 9:e104899. <https://doi.org/10.1371/journal.pone.0104899>.
33. Janvier F, Jeannot K, Tesse S, Robert-Nicoud M, Delacour H, Rapp C, Merens A. 2013. Molecular characterization of blaNDM-1 in a sequence type 235 *Pseudomonas aeruginosa* isolate from France. *Antimicrob Agents Chemother* 57:3408–3411. <https://doi.org/10.1128/AAC.02334-12>.
34. Jovic B, Lepsanovic Z, Begovic J, Rakonjac B, Perovanovic J, Topisirovic L, Kojic M. 2013. The clinical isolate *Pseudomonas aeruginosa* MMA83 carries two copies of the blaNDM-1 gene in a novel genetic context. *Antimicrob Agents Chemother* 57:3405–3407. <https://doi.org/10.1128/AAC.02312-12>.
35. He T, Wang R, Liu D, Walsh TR, Zhang R, Lv Y, Ke Y, Ji Q, Wei R, Liu Z, Shen Y, Wang G, Sun L, Lei L, Lv Z, Li Y, Pang M, Wang L, Sun Q, Fu Y, Song H, Hao Y, Shen Z, Wang S, Chen G, Wu C, Shen J, Wang Y. 2019. Emergence of plasmid-mediated high-level tetracycline resistance genes in animals and humans. *Nat Microbiol* 4:1450–1456. <https://doi.org/10.1038/s41564-019-0445-2>.
36. Lee CA, Babic A, Grossman AD. 2010. Autonomous plasmid-like replication of a conjugative transposon. *Mol Microbiol* 75:268–279. <https://doi.org/10.1111/j.1365-2958.2009.06985.x>.
37. Carraro N, Poulin D, Burrus V. 2015. Replication and active partition of integrative and conjugative elements (ICEs) of the SXT/R391 family: the line between ICEs and conjugative plasmids is getting thinner. *PLoS Genet* 11:e1005298. <https://doi.org/10.1371/journal.pgen.1005298>.
38. Miyazaki R, Yano H, Sentchilo V, van der Meer JR. 2018. Physiological and transcriptome changes induced by *Pseudomonas putida* acquisition of an integrative and conjugative element. *Sci Rep* 8:5550. <https://doi.org/10.1038/s41598-018-23858-6>.
39. CLSI. 2019. Performance standards for antimicrobial susceptibility testing, 29th ed. CLSI supplement M100. Clinical and Laboratory Standards Institute, Wayne, PA.
40. Wick RR, Judd LM, Gorrie CL, Holt KE. 2017. Unicycler: resolving bacterial genome assemblies from short and long sequencing reads. *PLoS Comput Biol* 13:e1005595. <https://doi.org/10.1371/journal.pcbi.1005595>.
41. Walker BJ, Abeel T, Shea T, Priest M, Abouelliel A, Sakthikumar S, Cuomo CA, Zeng Q, Wortman J, Young SK, Earl AM. 2014. Pilon: an integrated tool for comprehensive microbial variant detection and genome assembly improvement. *PLoS One* 9:e112963. <https://doi.org/10.1371/journal.pone.0112963>.
42. Zankari E, Fasman H, Cosentino S, Vestergaard M, Rasmussen S, Lund O, Aarestrup FM, Larsen MV. 2012. Identification of acquired antimicrobial resistance genes. *J Antimicrob Chemother* 67:2640–2644. <https://doi.org/10.1093/jac/dks261>.
43. Bi D, Xu Z, Harrison EM, Tai C, Wei Y, He X, Jia S, Deng Z, Rajakumar K, Ou HY. 2012. ICEberg: a web-based resource for integrative and conjugative elements found in Bacteria. *Nucleic Acids Res* 40:D621–D626. <https://doi.org/10.1093/nar/gkr846>.
44. Zhang Z, Schwartz S, Wagner L, Miller W. 2000. A greedy algorithm for aligning DNA sequences. *J Comput Biol* 7:203–214. <https://doi.org/10.1089/10665270050081478>.
45. Sullivan MJ, Petty NK, Beatson SA. 2011. Easyfig: a genome comparison visualizer. *Bioinformatics* 27:1009–1010. <https://doi.org/10.1093/bioinformatics/btr039>.
46. Hua X, Zhang L, Moran RA, Xu Q, Sun L, van Schaik W, Yu Y. 2020. Cointegration as a mechanism for the evolution of a KPC-producing multidrug resistance plasmid in *Proteus mirabilis*. *Emerg Microbes Infect* 9:1206–1218. <https://doi.org/10.1080/22221751.2020.1773322>.
47. San Millan A, Heilbron K, MacLean RC. 2014. Positive epistasis between co-infecting plasmids promotes plasmid survival in bacterial populations. *ISME J* 8:601–612. <https://doi.org/10.1038/ismej.2013.182>.
48. Hua X, Chen Q, Li X, Yu Y. 2014. Global transcriptional response of *Acinetobacter baumannii* to a subinhibitory concentration of tetracycline. *Int J Antimicrob Agents* 44:337–344. <https://doi.org/10.1016/j.ijantimicag.2014.06.015>.
49. McClure R, Balasubramanian D, Sun Y, Bobrovskyy M, Sumbly P, Genco CA, Vanderpool CK, Tjaden B. 2013. Computational analysis of bacterial RNA-Seq data. *Nucleic Acids Res* 41:e140. <https://doi.org/10.1093/nar/gkt444>.
50. Robinson MD, McCarthy DJ, Smyth GK. 2010. edgeR: a Bioconductor package for differential expression analysis of digital gene expression data. *Bioinformatics* 26:139–140. <https://doi.org/10.1093/bioinformatics/btp616>.
51. Wickham H. 2016. ggplot2: elegant graphics for data analysis. Springer-Verlag, New York, NY. <https://ggplot2.tidyverse.org>.